Statistics of current-activity fluctuations in asymmetric flow with exclusion

R. B. Stinchcombe[1,*] and S. L. A. de Queiroz[1,2,†]

[1]*Rudolf Peierls Centre for Theoretical Physics, University of Oxford, 1 Keble Road, Oxford OX1 3NP, United Kingdom*

[2]*Instituto de Física, Universidade Federal do Rio de Janeiro, Caixa Postal 68528, 21941-972 Rio de Janeiro RJ, Brazil*

(Received 3 February 2012; published 10 April 2012)

We consider steady-state current activity statistics for the one-dimensional totally asymmetric simple exclusion process. With the help of the known operator algebra (for general open boundary conditions), as well as general probabilistic concepts (for the periodic case), we derive and evaluate closed-form expressions for the lowest three moments of the probability distribution function. These are confirmed, to excellent degree of accuracy, by numerical simulations. Further exact expressions and asymptotic approximations are provided for probability distributions and generating functions.

DOI: 10.1103/PhysRevE.85.041111 PACS number(s): 05.40.−a, 02.50.−r, 05.70.Fh

I. INTRODUCTION

The one-dimensional totally asymmetric simple exclusion process (TASEP) is a biased diffusion process for particles with hard-core repulsion [1–5]. This model exhibits many nontrivial properties, and is considered a paradigm in the field of nonequilibrium phenomena. While a large number of exact results are known for the steady-state, ensemble-averaged values of relevant quantities, such as the system-wide current and global density, the study of the corresponding fluctuations has proved to be rather more intricate. To quote only a few relevant developments, exact expressions for the diffusion constant were found for systems with periodic (PBC) [6] and open [7] boundary conditions (BC); the full probability distribution function (PDF) of current fluctuations was similarly considered for both PBC [8] and open [9] BC. Very recently, a number of new results have been found for current fluctuations in systems with open BC [10–13].

In this paper, we investigate steady-state current-activity fluctuations in the one-dimensional TASEP for both periodic and open boundary conditions. It is important to recall at the outset that the current *activity* is not identical to the standard current (although the first moments of the respective distributions coincide). As explained in detail below, the former quantity is *static*, in this sense akin to the instantaneous (local or global) particle density, while the latter is a dynamic one. Our results extend and complement earlier analytic work on the joint current-density distribution for the TASEP [14,15].

For the problem of flow with exclusion, the time evolution of the $1+1$ dimensional TASEP is the fundamental discrete model. The particle number n_ℓ at lattice site ℓ can be 0 or 1, and the forward hopping of particles is only to an empty adjacent site. The current across the bond from ℓ to $\ell+1$ depends also on the stochastic attempt rate p_ℓ associated with it and is thus given by $J_{\ell,\ell+1} = p_\ell\, n_\ell(1-n_{\ell+1})$. For the homogeneous case of $p_\ell = p$ which is considered here, one can effectively make $p=1$ in numerical simulations, provided that the inherent stochasticity of the process is kept, via, for example, random selection of site occupation update [16]. This amounts to a trivial renormalization of the time scale, and is the procedure followed in all numerical work reported in this paper.

For PBC, the main parameter is the fixed density, which is uniform in the steady state. With open boundary conditions, one has the following externally imposed parameters: the injection (attempt) rate α at the left end, and the ejection rate β at the right one. The phase diagram in α-β parameter space is known exactly, as well as many other steady-state properties [1–5,14,15,17,18].

In the open boundary case, both current and global (position-averaged) particle density are fluctuating quantities (as opposed to the case with PBC for which the density is fixed). On the other hand, while continuity dictates that the average stationary current on every bond must be the same, steady-state density profiles may be nonuniform [3].

For PBC, the total (instantaneous) activity A within the system is defined as the number of bonds that can facilitate a transition of a particle in the immediate future. Thus, it equals the number of pairs of neighboring sites that have a particle to the left and a hole to the right [14,15]. For systems with open BC, an alternative definition includes also the injection and ejection bonds at the system's ends, although these have to be weighted by the respective injection and ejection rates α and β. In the following, for open BC we always include the contributions given by the latter bonds, unless explicitly stated otherwise.

Thus, for an L-site system with PBC, one has

$$A = \sum_{\ell=1}^{L} n_\ell\,(1-n_{\ell+1}) \quad \text{(PBC)} \tag{1}$$

(with $n_{L+1} \equiv n_1$), while for the open BC case (L sites and $L+1$ bonds, including the injection and ejection ones), one has

$$A = \alpha\,(1-n_1) + \sum_{\ell=1}^{L-1} n_\ell\,(1-n_{\ell+1}) + \beta\, n_L \quad \text{(open BC)}. \tag{2}$$

The activity is, therefore, a snapshot of the system at a given moment in its evolution; in this sense, it is as much of a static quantity as, for example, the instantaneous global density. By contrast, the current is a dynamic object, as it

*r.stinchcombe1@physics.ox.ac.uk

†sldq@if.ufrj.br

reflects the stochastically determined particle displacements which actually take place during a unit time interval.

The detailed balance measure used here for the PBC case, and the operator algebra used for open BC, apply to the steady state [5,6,14,15], thus they naturally yield the activity; although they can be extended to deal with static measures of dynamic quantities such as the diffusion constant [6,7] and more general aspects [4,19], we do not attempt similar developments here.

The qualitative distinction between activity and current has the consequence, upon the (properly normalized) moments of the PDFs of the two quantities, that while their first moments (averages) coincide, higher cumulants differ. For A as defined in Eqs. (1) and (2) one has, respectively,

$$J = \frac{1}{L}\,\langle A\rangle \quad \text{(PBC)}, \tag{3}$$

$$J = \frac{1}{L+1}\,\langle A\rangle \quad \text{(open BC)}, \tag{4}$$

where J is the average steady-state current through any bond in the system. Equality of averages can be understood by recalling that successive steady-state snapshots (activity configurations) are generated via the intervening particle hoppings, which constitute realizations of the system's current. In our simulations, we have verified that this property holds, to within numerical accuracy, in all cases investigated here. However, the connection at this level is not sufficient to warrant equality of higher moments of the PDFs. Here, we consider the fluctuations of the *global*, *instantaneous* activity [14,15], as opposed to the *local*, *integrated* current, which is the subject of many extant works [7–13].

Section II gives the theoretical approach used in this work. It first addresses open boundary cases with $\alpha+\beta=1$ and then general α, β, and then treats PBC. In Sec. III, the results of numerical simulations are given, first for open BC and then for PBC. In Sec. IV, we provide a global discussion of the second and third cumulants of the activity PDFs, everywhere on the α-β plane (for open BC); finally, concluding remarks are made.

II. THEORY

A. Open boundary conditions with $\alpha+\beta=1$

For open boundary conditions, steady-state configurations are typically highly correlated. So, when (as in the pioneering work of Ref. [3]) such configurations are written as strings of variables D and E (D and E representing particle and vacancy, respectively), these variables have to be operators, with an algebra ($D+E=DE$) consistent with the steady-state properties. In the special case $\alpha+\beta=1$, the correlations disappear [3] (configuration probabilities factorize, corresponding to a product measure) and D and E can be taken as c numbers d and e, respectively, equal to the steady-state averages $\langle n_\ell\rangle$ and $\langle 1-n_\ell\rangle$. Consequently, along the $\alpha+\beta=1$ line, these averages are independent of ℓ [3]; consistency with probability normalization ($d+e=1$) and current conservation ($e\alpha = de = d\beta$) thus implies $e=\beta$, $d=\alpha$.

The factorization of probabilities for variables on different sites makes this case the easiest to begin with. However, different bonds share a site variable if they are adjacent, and that makes the calculation of activity statistics beyond the first moment nontrivial even in this case. The average activity $\langle A\rangle$ is unaffected by the shared variable on adjacent bonds since it is the average of a sum of terms, each of which contains independent site variables and so has a factorizing average. So, in this case, from Eq. (2) one has

$$\langle A\rangle = (L+1)\,\alpha\beta \quad (\alpha+\beta=1). \tag{5}$$

Already in the second moment $\langle A^2\rangle$ the effect of correlations are present, making it different from $\langle A\rangle^2$. To obtain any moment, and also the probability distribution, we consider the generating function

$$\langle e^{\lambda A}\rangle = \left\langle e^{\lambda\alpha\,(1-n_1)} \left(\prod_{\ell=1}^{L-1} e^{\lambda\, n_\ell\,(1-n_{\ell+1})}\right) e^{\lambda\beta\, n_L}\right\rangle. \tag{6}$$

Logarithmic derivatives of $\langle e^{\lambda A}\rangle$ give the cumulants C_n of A. The probabilities $P(A_i)$ of the discrete possible outcomes A_i for A are the coefficients in the terms proportional to $e^{\lambda A_i}$ in the expansion of the generating function. The average in Eq. (6) does not factorize because of the correlation of adjacent bond variables. The following method, involving a transfer matrix along the chain, easily handles that.

Defining $\zeta_\ell \equiv 1-n_\ell$, since each ζ_ℓ takes values (0,1) with respective probabilities (α,β), the average in Eq. (6) can be obtained by summing over the possible configurations of each variable in turn, starting, say, with $\ell=1$ and working along the chain to $\ell=L$. Using sums over the ζ_ℓ variables, with their weights $p(\zeta_\ell)$ ($=\alpha$ or β), the first step involves $\Sigma_{\zeta_1=0,1}\,p(\zeta_1)\,e^{\lambda\alpha\,\zeta_1}\,e^{\lambda\,(1-\zeta_1)\,\zeta_2} = \alpha\,e^{\lambda\,\zeta_2} + \beta\,e^{\lambda\alpha}$. This result can be written in the linear form $(b_2+c_2\,\zeta_2)$ where $b_2=\alpha+\beta e^{\lambda\alpha}$ and $c_2=\alpha\,(e^\lambda-1)$. The sums over the next variables then produce similar forms, where the relationship between successive ones is provided by

$$b_{\ell+1}+c_{\ell+1}\,\zeta_{\ell+1} = \sum_{\zeta_\ell=1,0} p(\zeta_\ell) e^{\lambda(1-\zeta_\ell)\zeta_{\ell+1}}(b_\ell+c_\ell\zeta_\ell). \tag{7}$$

This is the same as the action of the transfer matrix

$$T = \begin{pmatrix} \alpha+\beta & \beta \\ \alpha\gamma & 0 \end{pmatrix} \tag{8}$$

on the vector $\binom{b_\ell}{c_\ell}$, where $\gamma = e^\lambda - 1$. The consequence is

$$\begin{aligned}\langle e^{\lambda A}\rangle &= \sum_{\zeta_L} p(\zeta_L)\,(b_L + c_L\,\zeta_L)\,e^{\lambda\beta\,(1-\zeta_L)} \\ &= (\alpha\,e^{\lambda\beta}+\beta\beta)\,T^{L-1}\begin{pmatrix} b_1 \\ c_1\end{pmatrix},\end{aligned} \tag{9}$$

where, from $e^{\alpha\zeta_1} = b_1 + c_1\,\zeta_1$, $b_1=1$, $c_1 = e^{\lambda\alpha}-1$.

This is readily evaluated using the representation in which T is diagonal, with the result

$$\langle e^{\lambda A}\rangle = a_+\,\mu_+^{L-1} + a_-\,\mu_-^{L-1}\,, \tag{10}$$

where

$$\mu_\pm = \tfrac{1}{2}[1 \pm \sqrt{(\alpha-\beta)^2+4\alpha\beta\,e^\lambda}] \equiv \tfrac{1}{2}[1\pm\varphi] \tag{11}$$

are the two eigenvalues of T, and the coefficients a_+, a_- are also known functions of α, β, γ (given in Appendix A).

This result provides the nth cumulant C_n of A via

$$C_n = \left(\frac{\partial}{\partial\lambda}\right)^n \ln\langle e^{\lambda A}\rangle\Big|_{\lambda=0}. \tag{12}$$

From Eqs. (10) and (11), for large L one has

$$\ln\langle e^{\lambda A}\rangle \approx L\,\ln\mu_+ + \mathcal{O}(1). \tag{13}$$

Consequently, the asymptotic large-L values of the first few cumulants are

$$C_1 = \langle A\rangle \approx L\,\frac{\partial}{\partial\lambda}\ln\mu_+\Big|_{\lambda=0} = L\,\alpha\beta + \mathcal{O}(1), \tag{14}$$

$$C_2 = \langle A^2\rangle - \langle A\rangle^2 \approx L\,\alpha\beta\,[1-3\alpha\beta] + \mathcal{O}(1), \tag{15}$$

$$C_3 = \langle A^3\rangle - 3\langle A\rangle\langle A^2\rangle + 2\langle A\rangle^3 \approx L\,\alpha\beta\,[1-9\alpha\beta+20(\alpha\beta)^2] + \mathcal{O}(1). \tag{16}$$

Thus, the skewness [20] $S \equiv C_3/C_2^{3/2}$ is of order $L^{-1/2}$ for large L.

The special case $\alpha=\beta=1/2$ is simple and instructive. There, the above leading large-L results for C_3 and skewness reduce to zero, which turns out to be exactly true for any L: for $\alpha=\beta=1/2$, the coefficient a_- vanishes and the full result from Eqs. (10) and (11) (exact for any L) is

$$\langle e^{\lambda A}\rangle = e^{\lambda/2}\left[\tfrac{1}{2}(1+e^{\lambda/2})\right]^{L-1}. \tag{17}$$

From this it is easy to verify that $C_3 = S \equiv 0$, and that $C_1 = (L+1)/4$, $C_2 = (L-1)/16$. The corresponding general L exact results obtained from Eqs. (10) and (11) for any α,β with $\alpha+\beta=1$ are given in Appendix A, together with validity conditions for the large-L results in Eqs. (14)–(16).

For $\alpha=\beta=1/2$, the generating function result [Eq. (17)] can be expanded in the form

$$\langle e^{\lambda A}\rangle = 2^{-(L-1)}\sum_{n=0}^{L-1} {}_{L-1}C_n\, e^{\frac{\lambda}{2}(n+1)}, \tag{18}$$

corresponding to a binomial distribution of probabilities $P(A_m = m/2) = 2^{-(L-1)}\,{}_{L-1}C_{m-1}$ for the possible outcomes $m/2$, $1\leqslant m\leqslant L$, of the activity. For general α, β (still with $\alpha+\beta=1$), the possible outcomes for A will obviously be linear combinations of α, β, and integers. Their distribution, resulting from Eqs. (10) and (11), has (for $\alpha\neq\beta$, where a_- is nonvanishing) a "discreteness alternation." This is a direct consequence of Eqs. (10) and (11), as can be seen from the following alternative form:

$$\langle e^{\lambda A}\rangle = 2^{-(L-1)}\sum_{n=0}^{L-1} {}_{L-1}C_n\,\varphi^n[a_+ + (-1)^n a_-]. \tag{19}$$

We conclude this part on activity statistics for $\alpha+\beta=1$ by briefly commenting on local fluctuations. The product measure makes these trivial for this case. So, the injection current activity (from $\alpha\zeta_1$) is α or 0, with probabilities β and α, respectively. The local activity for the ejection current $[\,\beta\,(1-\zeta_L)\,]$ and for the internal current $[\,(1-\zeta_\ell)\,\zeta_{\ell+1} = A_{\ell,\ell+1}\,]$ across any specified bond similarly have binary distributions, with (outcomes) (respective probabilities) being $(\beta,0)$ (α,β) and $(1,0)$ $(\alpha\beta, 1-\alpha\beta)$, respectively. So, for example, $\langle A_{\ell,\ell+1}\rangle = \alpha\beta$, $\langle A_{\ell,\ell+1}\rangle^2 = \langle A_{\ell,\ell+1}\rangle^3 = \alpha\beta^3$, independent of ℓ, and the consequent skewness is $(\beta-\alpha)(\alpha\beta)^{-1/2}$.

B. Open boundary conditions with general α, β

1. *Moments of the current activity*

For general α, β, one must make full use of the steady-state operator algebra [3] to take care of the absence of product measure. In this section, we derive expressions for low moments of the activity. We exploit the representation of configurations, and their probabilities, using strings of operators D and E representing, respectively, particle or vacancy at a site. Configurations are specified using the variables ζ_ℓ introduced in Sec. II A. The probability of the configuration $\{\zeta_\ell\}$ for L sites is given, through the associated operator string $S(\{\zeta_\ell\}) = \prod_{j=1}^{L}[(1-\zeta_j)\,D + \zeta_j\,E]$, as

$$P(\{\zeta_\ell\}) = \frac{\langle W|S(\{\zeta_\ell\})\,|V\rangle}{Z_L}, \quad \text{with} \quad Z_L \equiv \langle W|C^L\,|V\rangle. \tag{20}$$

Here, $C \equiv D+E$ represents both possibilities (occupied or vacant) at a given site, and the vectors $\langle W|$ and $|V\rangle$ are such that

$$\langle W|\,\alpha E = \langle W|\,, \quad \beta D\,|V\rangle = |V\rangle. \tag{21}$$

Equations (21) follow from the balance between the current $\Lambda \equiv DE$ across any internal bond and the injection or ejection current (at the left or right boundary), using the operator algebra steady-state relation $\Lambda = C$. Using Eq. (2), the nth moment of the total activity is given by

$$\langle A^n\rangle = \sum_{\{\zeta_j\}}\left(\alpha\zeta_1 + \sum_{\ell=1}^{L-1}(1-\zeta_\ell)\zeta_{\ell+1} + \beta(1-\zeta_L)\right)^n \times \frac{\langle W|\prod_{j=1}^{L}[(1-\zeta_j)\,D+\zeta_j\,E]\,|V\rangle}{Z_L}. \tag{22}$$

Consider, for example, the simple case $n=1$. There, the contribution from $(1-\zeta_\ell)\zeta_{\ell+1}$ is nonzero only for $1-\zeta_\ell=1$, $\zeta_{\ell+1}=1$, the associated probability of which is (using $\Lambda \equiv DE = C$)

$$\frac{\langle W|C^{\ell-1}\,DE\;C^{L-(\ell+1)}|V\rangle}{Z_L} = \frac{Z_{L-1}}{Z_L}. \tag{23}$$

Correspondingly, using Eq. (21), the nonzero contributions α from $\alpha\zeta_1$ and β from $\beta(1-\zeta_L)$ occur with respective probabilities $\alpha^{-1}\,Z_{L-1}/Z_L$ and $\beta^{-1}\,Z_{L-1}/Z_L$, making

$$\langle A\rangle = (L+1)\,\frac{Z_{L-1}}{Z_L}. \tag{24}$$

This is the standard result generalizing Eq. (14) for $\alpha+\beta=1$, where $Z_L = (\alpha\beta)^{-L}$.

As in Sec. II A, complications arise in higher moments from the shared variable in adjacent bonds. For $\alpha+\beta=1$, the transfer-matrix approach overcame these. That method is ruled out by the noncommuting variables in the present general case. Instead, the following direct method can be used for low n.

For $n=2$, Eq. (22) includes the product of bond terms $(\sum_{\ell=1}^{L-1}(1-\zeta_\ell)\zeta_{\ell+1})\,(\sum_{m=1}^{L-1}(1-\zeta_m)\zeta_{m+1})$. For $m-\ell\neq 0,1$

in the double sum the sites involved are distinct, which simplifies the averages occurring. For example, for $m > \ell + 1$, the average is

$$\frac{\langle W|C^{\ell-1}\,DE\;C^{m-\ell-2}\,DE\,C^{L-(m+1)}|V\rangle}{Z_L} = \frac{Z_{L-2}}{Z_L}. \quad (25)$$

This result applies for any ℓ, m satisfying $m > \ell + 1$, or $\ell > m + 1$ [altogether $(L-2)(L-3)$ terms of the double sum]. For each of the $L-1$ terms with $\ell = m$, the product of bond variables is $[(1-\zeta_\ell)\zeta_{\ell+1}]^2 = (1-\zeta_\ell)\zeta_{\ell+1}$, having average $\langle W|C^{\ell-1}\,\Lambda\;C^{L-(\ell+1)}|V\rangle/Z_L = Z_{L-1}/Z_L$.

For the $2(L-2)$ terms with $\ell = m \pm 1$, the product of variables includes both a $1-\zeta$ and a ζ for the shared site, the product of which is zero. Hence, for the part $A' = \sum_{\ell=1}^{L-1}(1-\zeta_\ell)\zeta_{\ell+1}$ of the activity coming from just the internal bonds,

$$\langle A'^2\rangle = (L^2 - 5L + 6)\,\frac{Z_{L-2}}{Z_L} + (L-1)\,\frac{Z_{L-1}}{Z_L}. \quad (26)$$

Including also the injection and ejection contributions gives

$$\begin{aligned}\langle A^2\rangle &= \langle[\alpha\zeta_1 + A' + \beta(1-\zeta_L)]\rangle^2 \\ &= \langle A'^2\rangle + \langle\alpha^2\zeta_1 + 2\alpha\beta\zeta_1(1-\zeta_L) \\ &\quad + \beta^2(1-\zeta_L)\rangle + \langle 2[\alpha\zeta_1 + \beta(1-\zeta_L)]A'\rangle \\ &= \langle A'^2\rangle + (\alpha+\beta)\,\frac{Z_{L-1}}{Z_L} + 2\,\frac{Z_{L-2}}{Z_L} + 2\Gamma, \end{aligned} \quad (27)$$

where

$$\begin{aligned}\Gamma &= \left\langle \left\{ \alpha\zeta_1(1-\zeta_1)\zeta_2 + \alpha\zeta_1 \sum_{\ell=2}^{L-1}(1-\zeta_\ell)\zeta_{\ell+1} + (1-\zeta_{L-1}) \right.\right. \\ &\quad \left.\left. \times\,\zeta_L\,\beta(1-\zeta_L) + \beta(1-\zeta_L)\sum_{\ell=1}^{L-2}(1-\zeta_\ell)\zeta_{\ell+1} \right\}\right\rangle \\ &= 2(L-2)\,\frac{Z_{L-2}}{Z_L}. \end{aligned} \quad (28)$$

The case $n = 3$ is in principle a straightforward generalization of the above. However, the $\langle A'^3\rangle$ part of it is considerably more complicated. Details of the evaluation are given in Appendix B.

The collected results for the first three moments of both A and A' are

$$\begin{aligned} n = 1\text{:}\quad \langle A\rangle &= (L+1)\,\frac{Z_{L-1}}{Z_L}, \\ \langle A'\rangle &= (L-1)\,\frac{Z_{L-1}}{Z_L}; \end{aligned} \quad (29)$$

$$\begin{aligned} n = 2\text{:}\quad \langle A^2\rangle &= L(L-1)\,\frac{Z_{L-2}}{Z_L} + (L-1+\alpha+\beta)\,\frac{Z_{L-1}}{Z_L}, \\ \langle A'^2\rangle &= (L-2)(L-3)\,\frac{Z_{L-2}}{Z_L} + (L-1)\,\frac{Z_{L-1}}{Z_L}; \end{aligned} \quad (30)$$

$$\begin{aligned} n = 3\text{:}\quad \langle A^3\rangle &= (L-1)(L-2)(L-3)\,\frac{Z_{L-3}}{Z_L} \\ &\quad + 3(L-1)(L-2+\alpha+\beta)\,\frac{Z_{L-2}}{Z_L} \\ &\quad + (L-1+\alpha^2+\beta^2)\,\frac{Z_{L-1}}{Z_L}, \\ \langle A'^3\rangle &= (L-3)(L-4)(L-5)\,\frac{Z_{L-3}}{Z_L} \\ &\quad + 3(L-2)(L-3)\,\frac{Z_{L-2}}{Z_L} + (L-1)\,\frac{Z_{L-1}}{Z_L}. \end{aligned} \quad (31)$$

The functions Z_L are available from Ref. [3] or by using the generating function method of Refs. [14,15]. The general expression is

$$Z_L = \sum_{\ell=1}^{L} \frac{\ell\,(2L-\ell-1)!}{L!\,(L-\ell)!} \sum_{k=0}^{\ell} \alpha^{-k}\,\beta^{k-\ell}. \quad (32)$$

Equation (32) reduces to simple closed-form expressions in the cases

(i) $\alpha + \beta = 1$:

$$Z_L = (\alpha\beta)^{-L}, \quad (33)$$

(ii) $\alpha = \beta = 1$:

$$Z_L = \frac{(2L+2)!}{(L+2)!\,(L+1)!}. \quad (34)$$

From Eqs. (29)–(31) and (34), one can show that, for $\alpha = \beta = 1$ and large L, the skewness S (of the distribution for A) varies as

$$S = 9L^{-5/2}\,[1 + \mathcal{O}(L^{-1})] \quad (\alpha = \beta = 1). \quad (35)$$

In Sec. III B, we describe numerical simulations performed for the cases covered by Eqs. (33) and (34). We return to the general α, β case, using Eq. (32), in Sec. IV.

2. *Activity distribution: I*

This section is concerned with the internal bond activity distribution for general α, β. We again use the internal bond current-activity operator $\Lambda = DE$, and $C = D + E$, which represents both possible single-site configurations.

For n successive sites, C^n represents all possible configurations; we generalize this by representing by (C^n) the subset which contains no Λ's. Hereafter, in this section the round bracket pair $(\cdots)$, when enclosing a string of C's or a linear combination of such strings, will represent the formal property of picking out the subset containing no Λ's. Then, by definition, $(C^{r_0})\,\Lambda\,(C^{r_1})\,\Lambda\,(C^{r_2})\,\Lambda\,\ldots\,(C^{r_{n-1}})\,\Lambda\,(C^{r_n})$ contains many configurations, all having n active internal bonds (total internal activity $A' = n$), from the n Λ's in a run of $L = 2n + \sum_{m=0}^{n} r_m$ sites. Then,

$$\mathcal{S}_{L,A'}\{(C^r)\} = \sum_{r_0\geqslant 0}\cdots\sum_{r_{A'}\geqslant 0}(C^{r_0})\,\Lambda\,\ldots\,(C^{r_{A'-1}})\,\Lambda\,(C^{r_{A'}}), \quad (36)$$

with $r_0 + r_1 + \cdots + r_{A'} = L - 2A'$, contains all configurations with internal activity A' in an L-site system. So, in such a system the probability of internal current activity A' is

$$P_L(A') = Z_L^{-1}\,\langle W|\,\mathcal{S}_{L,A'}\{(C^r)\}\,|V\rangle. \quad (37)$$

From their definitions, it follows that (C^n) and $\mathcal{S}_{n,A'}$ are related by

$$(C^n) = C^n - \sum_{A'=1}^{[\frac{n}{2}]} \mathcal{S}_{n,A'}, \tag{38}$$

where $[\,X\,]$ denotes the integer part of X. The steady-state algebra relation $\Lambda = C$ then makes (C^n) a function of C only, so no lack-of-commutation difficulties arise and one finds that $\mathcal{S}_{L,A'}$ is the coefficient of $\gamma^{L-2A'}$ in the expansion of $C^{A'}(\frac{1}{1-\gamma C})^{A'+1}$. That makes $\mathcal{S}_L \equiv \sum_{A'=1} \mathcal{S}_{L,A'}$ the coefficient of γ^L in $S(\gamma)$, where

$$S(\gamma) = \left(\frac{1}{1-\gamma C}\right)^2 \gamma^2 C \left[1 - \gamma^2 C \left(\frac{1}{1-\gamma C}\right)\right]^{-1}. \tag{39}$$

Then, consideration of $\sum_{n=0}^{\infty} \gamma^n \mathcal{S}_n$ eventually gives the following reduction of the formal operation defined by $(\cdots)$:

$$\left(\frac{1}{1-\gamma C}\right) = \frac{1}{1 - C(\gamma - \gamma^2)}. \tag{40}$$

Hence, $\mathcal{S}_{L,A'}$ is the coefficient of $\gamma^{L-2A'}$ in

$$S'(\gamma, A') = C^{A'}\,[1 - C(\gamma - \gamma^2)]^{-(A'+1)}. \tag{41}$$

The required coefficient can be found by the expansion of the function of C in powers of $(\gamma - \gamma^2)$, and then using the binomial expansion of each power of $(1-\gamma)$ occurring. Taking the matrix element $\langle W| \cdots |V\rangle$ of the resulting C-dependent coefficient and using the definition of Z_N then provides the following exact result for the internal activity distribution:

$$P_L(A') = \frac{1}{Z_L} \sum_{s=0}^{[\frac{L-2A'}{2}]} Z_{L-A'-s} (-1)^s \frac{(L-A'-s)!}{A'!s!(L-2A'-2s)!}. \tag{42}$$

An alternative expansion strategy from Eq. (41) onward is available for the special case $\alpha + \beta = 1$. Because the operators reduce to c numbers in this case, C in that equation becomes $(\alpha\beta)^{-1}$, so $[1 - C(\gamma - \gamma^2)]$ becomes $(\alpha\beta)^{-1}(\gamma - \gamma_+)(\gamma - \gamma_-)$ where $\gamma_\pm = \frac{1}{2}(1 \pm \sqrt{1-4\alpha\beta}) = \alpha,\ \beta$ [the same as the eigenvalues $\mu_\pm(\lambda)$ of the transfer matrix of Sec. II A, at $\lambda = 0$].

In particular, $\gamma_+ = \gamma_- = \frac{1}{2}$ for $\alpha = \beta = \frac{1}{2}$, so it follows that

$$P_L(A') = 2^{-L}\ {}_{L+1}C_{2A'+1}. \tag{43}$$

For large L, where boundary current contributions to A are less by a factor $\mathcal{O}(1/L)$ from the total internal bond current contributions which comprise A', Eq. (43) becomes the same as the result from Eq. (18).

Although the method just presented applies for any α, β, it is not suitable for inclusion of boundary current contributions. We briefly proceed next to a more sophisticated approach to the current activity distribution, which is in no such way limited, and is related to previous work [14,15] on the joint distribution for number and current activity.

3. *Activity distribution: II; generating functions*

The method of Refs. [14,15] represented any microscopic configuration of N particles with internal activity A' in the L-site open boundary TASEP as a sequence of A' objects of form $D^{p_j} E^{h_j}$, $p_j, h_j \geqslant 1$, with $h_0 \geqslant 0$ E's to the left and $p_0 \geqslant 0$ D's to the right because of the possible injection and ejection. The operator string representation for the set of all such configurations is obtained by summing over all $\{h_j, p_j\}$ as specified above, subject to the additional constraints coming from specified L, N, and A':

$$\sum_{j=0}^{A'} (h_j + p_j) = L, \quad \sum_{j=0}^{A'} p_j = N. \tag{44}$$

$h_0 > 0$ (or $p_0 > 0$) corresponds to unit injection (or ejection) current activity, accounting for any difference between A' and A. The steady-state measure is then obtained from the $\langle W| \cdots |V\rangle$ matrix element of the operator string. This was reduced in Refs. [14,15] using a generalized version of the original operator algebra of Ref. [3].

We are now interested in just the activity distribution, for specific L, so the constraint on N drops out and the remaining constraints can be enforced using an integral representation of a δ function. The resulting expression for the total activity probability function $P_L(A)$ can then be reduced using the modified operator algebra of Refs. [14,15]. The result is that $P_L(A)$ is the coefficient of z^{L-2A} in

$$G(\alpha,\beta,A,z) = \frac{\alpha\beta}{Z_L^{\alpha\beta}} \frac{Z_A^{\alpha'\beta'}}{(z-\alpha)(z-\beta)(1-2z)^{2A}}, \tag{45}$$

where, in the numerator, $\alpha' = (\alpha - z)/(1-2z)$, $\beta' = (\beta - z)/(1-2z)$ replace α, β to obtain the "renormalized" version from the usual $Z_L \equiv Z_L^{\alpha\beta}$. Equivalently, the double-integral representation of Refs. [14,15] for the joint distribution $P_L(A,N)$ can be summed over N to provide the above form.

As well as giving rise to the renormalized $Z_A^{\alpha'\beta'}$, the modified algebra also gives a generating functional for $Z_L^{\alpha\beta}$; that can be exploited following Ref. [15] to give a direct form for the generating function $F_L^{\alpha\beta}(\lambda) \equiv \langle e^{\lambda A}\rangle$ as the coefficient of z^{L+1} in

$$U_L^{\alpha\beta}(z,\lambda) = \frac{4\alpha\beta}{Z_L^{\alpha\beta}} \left[\left\{2\alpha - 1 + \sqrt{(1-2z)^2 - 4z^2\,e^{\lambda}}\right\} \times \left\{2\beta - 1 + \sqrt{(1-2z)^2 - 4z^2\,e^{\lambda}}\right\}\right]^{-1}. \tag{46}$$

As expected, for $\alpha + \beta = 1$, the square bracket simplifies, and in the special case $\alpha + \beta = \frac{1}{2}$ it becomes a product of two factors linear in z. From this it is easy to recover Eq. (17) in Sec. II A.

The form obtained from Eq. (45) for the distribution function is not easy to simplify, except in the asymptotic large-L limit. There, saddle point integrals analogous to those in Refs. [14,15] give the activity distribution around its peak, apart from A-independent factors or others subdominant at large L.

The asymptotic results for all phases can alternatively be obtained by integrating out the density from the asymptotic

joint distribution results obtained in Refs. [14,15]. So, the activity distribution can be written for large L in the form

$$P_L(A) = \int_0^1 d\rho \, \exp[-L\, g(\rho, j)], \tag{47}$$

where for the low current phase with $\alpha < \beta$

$$\begin{aligned} g(\rho, j) = {} & 2j \ln j + (\rho - j)\ln(\rho - j) \\ & + (1 - \rho - j)\ln(1 - \rho - j) \\ & + \rho \ln[(1-\alpha)/\rho) + (1-\rho)\ln(\alpha/(1-\rho)], \end{aligned} \tag{48}$$

and for the maximal current phase $g(\rho, j)$ is of similar form but without the last two terms in Eq. (48).

The leading large-L approximation to Eq. (47), provided by the Laplace method {i.e., $\exp[-L\, g(\overline{\rho}, j)]$ where $\overline{\rho}(j)$ in $[0,1]$ minimizes g} gives, for example, a maximal current phase PDF independent of α and β, and the same as the Laplace result for the low current phase PDF at $\alpha = \beta = \frac{1}{2}$, which is consistent there with the general L result under Eq. (18).

Although of theoretical interest, the results for probability distributions obtained by the methods of the last two sections are of less value for detailed comparisons with numerical simulation results than the exact tractable expressions provided, for any L, in Sec. II B1 for low moments of the activity. See also Sec. IV.

C. Periodic boundary conditions

For PBC, the general ideas concerning operator strings, recalled in Sec. II B1, are again applicable. A number of simplifying features occur, aside from having a fixed number of particles in the system. From the very simple form of detailed balance equations applying in this case [6], for a given number M of particles all steady-state configurations $\mathcal{C}$ are equiprobable:

$$P(\mathcal{C}) = \frac{1}{{}_L C_M} \quad \text{(PBC)}. \tag{49}$$

We introduce the quantity

$$a_n \equiv \frac{(M-n)(L-M-n)}{L-n-1} \tag{50}$$

for $n = 0, 1, 2$, which will prove convenient in what follows.

With the notation established in Sec. II A, the average of the two-site function $(1-\zeta_\ell)\,\zeta_{\ell+1}$ is independent of ℓ, and proportional to the number of combinations in which site ℓ is occupied, site $\ell+1$ is vacant, and the remaining $M-1$ particles are distributed among the remaining $L-2$ sites. So,

$$\langle A \rangle = L\,\langle (1-\zeta_\ell)\,\zeta_{\ell+1}\rangle = \frac{{}_{L-2}C_{M-1}}{{}_L C_M} = a_0. \tag{51}$$

For $\langle A^2 \rangle$, similarly to the discussion in Sec. II B1, one needs averages of four-operator products, namely, $\mathcal{X}_{\ell m} \equiv \langle (1-\zeta_\ell)\,\zeta_{\ell+1}\,(1-\zeta_m)\,\zeta_{m+1}\rangle$. Three possibilities arise:

(i) $m = \ell$ [L terms]: $\mathcal{X}_{\ell\ell} = \langle (1-\zeta_\ell)\,\zeta_{\ell+1}\rangle = a_0/L$ [using $\zeta_\ell^2 = \zeta_\ell$, etc., and Eq. (51)];

(ii) $m = \ell \pm 1$ [$2L$ terms, from the ring geometry]: $\mathcal{X}_{\ell\,\ell\pm1} = 0$ [since $(1-\zeta_i)\,\zeta_i = 0$]; and

(iii) $m \neq \ell$, $\ell \pm 1$ [$L^2 - 3L$ terms]: contributions come from having sites ℓ, m occupied, $\ell+1$, $m+1$ vacant, and $M-2$ particles distributed among the remaining $L-4$ sites, so $\mathcal{X}_{\ell m} =_{L-4} {}_{L-2}C_{M-2}/{}_L C_M$.

Adding up (i)–(iii),

$$\langle A^2 \rangle = a_0\,(1 + a_1). \tag{52}$$

Details of the evaluation of $\langle A^3 \rangle$ are given in Appendix C. The result is

$$\langle A^3 \rangle = a_0\,(1 + 3a_1 + a_1\,a_2). \tag{53}$$

Introducing the variables $\rho \equiv M/L$; $\mu \equiv \rho(1-\rho)$; $\Lambda \equiv \mu L^2$; and $\widetilde{L} \equiv L - 1$, Eqs. (51)–(53) give the cumulants of the PDF in a form which evinces the expected particle-hole duality (invariance under $\rho \leftrightarrow 1-\rho$):

$$C_1 = \frac{\Lambda}{\widetilde{L}}, \tag{54}$$

$$C_2 = \frac{\Lambda\,[\Lambda - \widetilde{L}]}{\widetilde{L}^2\,(\widetilde{L}-1)}, \tag{55}$$

$$C_3 = \frac{\Lambda\,[4\Lambda^2 - \Lambda(\widetilde{L}^2 + 6\widetilde{L}) + \widetilde{L}^2\,(\widetilde{L}+2)]}{\widetilde{L}^3\,(\widetilde{L}-1)(\widetilde{L}-2)}. \tag{56}$$

For large L, the skewness S is given, to leading order in L^{-1}, by

$$S = \mu^{-1}\,(4\mu - 1)\,L^{-1/2}, \tag{57}$$

provided that $\mu \neq 1/4$, i.e., $\rho \neq 1/2$. In the latter case, consideration of higher-order terms shows that

$$S = 4\,L^{-5/2}\,[1 + \mathcal{O}(L^{-1})] \quad (\rho = 1/2). \tag{58}$$

III. NUMERICAL RESULTS

A. Introduction

We considered lattices with $L = 2^m$ sites. We found that the size range corresponding to $5 \leqslant m \leqslant 8$ is generally suitable to highlight L-dependent effects which vanish for $L \to \infty$, and for which we can provide accurate numerical checks of the theory developed in Secs. II A, II B1, and II C. On the other hand, such sizes are large enough to prevent lattice discreteness from playing a significant role [except for the discreteness alternation effect referred to above, in connection with Eq. (19), which for systems with open BC is a general feature unless $\alpha = \beta = \frac{1}{2}$ or 1]. For very low densities with PBC, for reasons explained in Sec. III C, we extended the size range up to $m = 11$.

A time step is defined as a set of L sequential update attempts, each of these according to the following rules: (1) select a site at random; (2a) if the chosen site is the rightmost one and is occupied, then (3a) eject the particle from it with probability β; alternatively, (2b) if the site is the leftmost one and is empty, then (3b) inject a particle onto it with probability α; finally, if neither (2a) nor (2b) is true, (2c) if the site is occupied and its neighbor to the right is empty, then (3c) move the particle. Thus, in the course of one time step, some sites may be selected more than once for examination, and some may not be examined at all.

For the various sets of α, β (for open BC) or values of ρ (for PBC) considered here [because of particle-hole duality, we take only $\alpha \leqslant \beta$ for the former case, and density $\rho \leqslant 1/2$

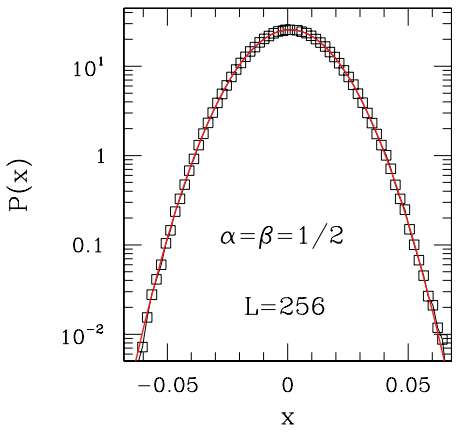

FIG. 1. (Color online) PDF for the reduced variable $x \equiv (A - \langle A \rangle)/(L+1)$ for $\alpha = \beta = 1/2$, $L = 256$ [see Eqs. (4) and (5)]. The points are from numerical simulations $N_{\rm sam} = 10^6$ samples. The full line is the binomial distribution given following Eq. (18).

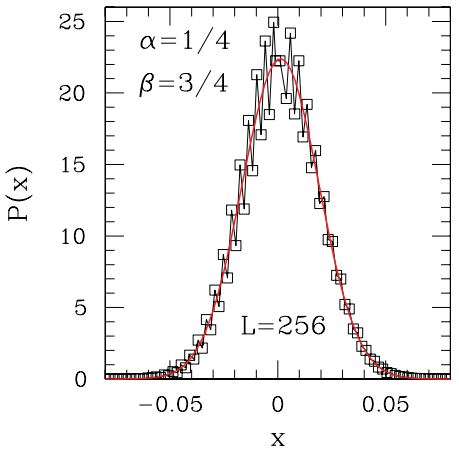

FIG. 2. (Color online) PDF for the reduced variable $x \equiv (A - \langle A \rangle)/(L+1)$ for $\alpha = 1/4$, $\beta = 3/4$, $L = 256$ [see Eqs. (4) and (5)]. The points are from numerical simulations $N_{\rm sam} = 10^6$ samples, and exhibit the discreteness alternation implied by Eq. (19). The full line is a Gaussian fit to the full set of simulation data.

for the latter], we ascertained that, starting from an initial random configuration of occupied sites (usually with overall density $\rho = 1/2$), $n_{\rm in} = 4000$ time steps was long enough for steady-state flow to be fully established, for all system sizes $L \leqslant 256$. This also applies to the special case of systems with PBC, $L \leqslant 2048$ and very low densities, examined in Sec. III C.

We collected steady-state current-activity data (typically $N_{\rm sam} = 10^5$–10^7 independent samples) to produce the respective PDFs. Accurate evaluation of their moments of nth order, $1 \leqslant n \leqslant 3$, involves running $N_{\rm set}$ independent sets of $N_{\rm sam}$ samples each; from the spread among the averaged moments for the distinct sets, one then estimates the root-mean-square (RMS) deviation of each relevant quantity. As is well known [21], such RMS deviations are essentially independent of $N_{\rm set}$ as long as $N_{\rm set}$ is not too small, and vary as $N_{\rm sam}^{-1/2}$. We generally took $N_{\rm set} = 10$.

Our results for the activity PDF are given in terms of the reduced variable $x \equiv (A - \langle A \rangle)/L_0$ [$L_0 = L + 1$ for open BC, or L for PBC], which, as a consequence of Eqs. (4) and (3), is suitable to highlight similarities and differences between the fluctuation statistics of activity and those of the standard current J.

B. Open boundary conditions

Initially, we consider the $\alpha + \beta = 1$ line. For the special point $\alpha = \beta = 1/2$, the considerations of Sec. II A [see also Eq. (43) in Sec. II B2] indicate that the PDF is a binomial function. Figure 1 shows the corresponding numerical simulation data for a system with $L = 256$ sites, together with the appropriate binomial distribution (which, for this value of L, is indistinguishable from a Gaussian function of a continuous variable). The fit between the two sets is indeed excellent.

On the $\alpha + \beta = 1$ line, the discreteness alternation effect associated with Eq. (19) is illustrated for $\alpha = 1/4$, $\beta = 3/4$ in Fig. 2. To avoid smoothing out of the effect, binning of the variable $x = (A - \langle A \rangle)/(L+1)$ must be carefully chosen; for the simulations reported in Fig. 2, we used bins of width $[2(L+1)]^{-1}$. In order to give higher resolution to the central part of the distribution, where the sawtooth pattern is quantitatively more significant, a linear scale has been used on the vertical axis of the figure. The Gaussian fit shown in Fig. 2 takes into account the full set of data, thus averaging over the oscillations. Remarkably, it produces a rather accurate fitted value $\Delta = 0.0178(3)$ for the corresponding width of the distribution (see Table I below for comparison).

Still on the $\alpha + \beta = 1$ line, for small α and large β (or, by particle-hole duality, for large α and small β), Eqs. (15) and (16) show that for large L the skewness S is positive

TABLE I. For systems with L sites, and α, β as specified, $\langle a_L \rangle \equiv \langle A \rangle/(L+1)$ is average current activity [normalized as in Eq. (4)]; $\Delta \equiv [\langle a_L^2 \rangle - \langle a_L \rangle^2]^{1/2}$; Th stands for results from theory [Eqs. (29)–(34)], and N for results of numerical simulations with $N_{\rm sam} = 10^6$, $N_{\rm set} = 10$ (see text).

L	Type	$\langle a_L \rangle$	Δ	Skew
		$\alpha = \beta = 1/2$		
64	Th	1/4	0.0305279 . . .	0
	N	0.24993(2)	0.030521(22)	− 0.0008(22)
128	Th	1/4	0.0218399 . . .	0
	N	0.24998(2)	0.021850(13)	− 0.0005(20)
256	Th	1/4	0.0155338 . . .	0
	N	0.24998(1)	0.015536(14)	0.0017(26)
		$\alpha = 1/4$, $\beta = 3/4$		
64	Th	3/16	0.0351324 . . .	0.01648 . . .
	N	0.18744(3)	0.035138(16)	0.0162(22)
128	Th	3/16	0.0250771 . . .	0.01134 . . .
	N	0.18747(3)	0.025080(17)	0.0118(22)
256	Th	3/16	0.0178161 . . .	0.00790 . . .
	N	0.18747(2)	0.017823(13)	0.0071(23)
		$\alpha = \beta = 1$		
64	Th	0.255814 . . .	0.0311221 . . .	0.000091968 . . .
	N	0.25583(4)	0.031183(20)	− 0.0017(19)
128	Th	0.252918 . . .	0.0220529 . . .	0.000016219 . . .
	N	0.25293(2)	0.022083(15)	0.0005(27)
256	Th	0.251462 . . .	0.0156096 . . .	0.000002864 . . .
	N	0.25146(2)	0.015618(8)	0.0008(12)

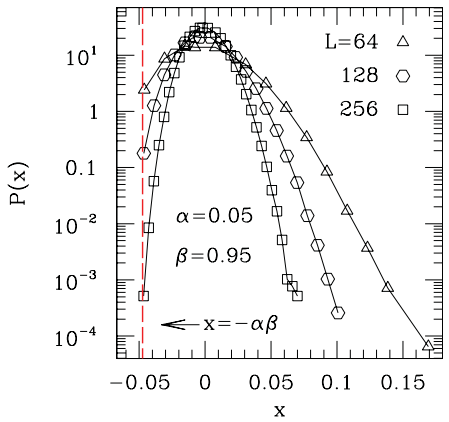

FIG. 3. (Color online) PDFs for the reduced variable $x \equiv (A - \langle A \rangle)/(L+1)$ for systems with open boundaries, $\alpha = 0.05$, $\beta = 1 - \alpha$, and sizes L as specified [see Eqs. (4) and (5)]. The points are from numerical simulations $N_{\rm sam} = 10^6$ samples. The dashed (red) line corresponds to the minimum allowed activity (see text).

and large, proportional to $(\alpha\beta)^{-1/2}$. The average activity being $\langle A \rangle = (L+1)\alpha\beta$, the minimum allowed value of the quantity $x = (A - \langle A \rangle)/(L+1)$ is $x_{\rm min} = -\alpha\beta$, i.e., $|x_{\rm min}| \ll 1$ for $\alpha \ll 1$, while positive values of $x \lesssim 0.5$ are permitted. This is illustrated in Fig. 3, where the discreteness alternation has been averaged out by using bins of width $(L+1)^{-1}$ for the x variable. The calculated values of S for the curves shown are $=0.4471\ldots$, $0.3158\ldots$, and $0.2232\ldots$, respectively, for $L = 64$, 128, 256 [see Eqs. (29)–(33)]. Large, positive skewness is expected to be a general feature also away from the $\alpha + \beta = 1$ line, anywhere for small α, large β (and the complementary region at large α, small β).

Away from the $\alpha + \beta = 1$ line, we report data for $\alpha = \beta = 1$, where the averaged moments are given by relatively simple expressions [see Eq. (34)]. The activity PDF is shown in Fig. 4, together with the result of a Gaussian fit to the data. Visual inspection indicates that the fit is of a similar quality to that for the $\alpha = \beta = 1/2$ data, displayed in Fig. 1. Indeed, according to Eqs. (29)–(31), (34), and (35), although

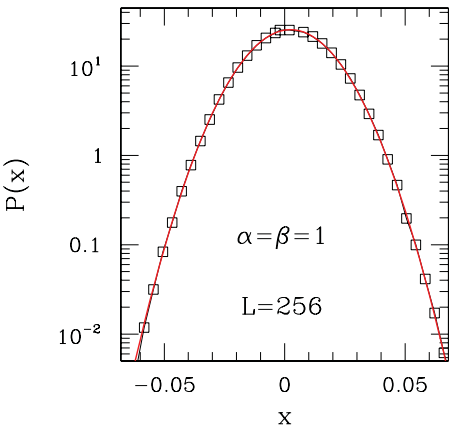

FIG. 4. (Color online) PDF for the reduced variable $x \equiv (A - \langle A \rangle)/(L+1)$ for $\alpha = \beta = 1$, $L = 256$ [see Eqs. (4), (29), and (34)]. The points are from numerical simulations $N_{\rm sam} = 10^6$ samples. The full line is a Gaussian fit to simulation data.

TABLE II. For systems with $L = 16$ sites, $\alpha = \beta = 1$, results for total activity: (a) including ($\langle A^n \rangle$) and (b) not including ($\langle A'^n \rangle$) injection and ejection bond contributions. $\Delta \equiv [\langle A^2 \rangle - \langle A \rangle^2]^{1/2}$; Th stands for results from theory [Eqs. (29)–(31), and (34)], and N for results of numerical simulations with $N_{\rm sam} = 10^7$, $N_{\rm set} = 10$ (see text).

Type	$\langle A \rangle$	Δ	Skew
		(a) $\langle A^n \rangle$	
Th	4.636363...	1.042933...	0.003006...
N	4.63655(37)	1.04286(25)	0.00295(69)
		(b) $\langle A'^n \rangle$	
Th	4.090909...	0.982518...	0.009706...
N	4.09113(34)	0.98246(12)	0.00959(34)

a nonvanishing skewness must be present in this case, it is quantitatively rather small for large L (see also Table I).

Results from numerical evaluation of the first three moments of the activity PDF, for the values of α, β discussed above, are given in Table I, together with the theoretical predictions summarized in Eqs. (29)–(34). The agreement is very good, except that accuracy for the skewness is comparatively low. This is especially true for $\alpha = \beta = 1$, in which case much narrower error bars would be needed in order to verify the rather small predicted values.

In order to clarify the latter point, we made long runs with $N_{\rm sam} = 10^7$ for $L = 16$ with $\alpha = \beta = 1$, evaluating both $\langle A^n \rangle$ and $\langle A'^n \rangle$ of Eqs. (29)–(31), with the results displayed in Table II. One can see that the numerical results clearly confirm the theoretical prediction for the skewness, within error bars.

C. Periodic boundary conditions

For systems with PBC, the $\rho \leftrightarrow 1 - \rho$ duality exhibited in Eqs. (54)–(56) ensures that all relevant aspects can be investigated by considering only, e.g., $\rho \leqslant 1/2$. We evaluated the first three moments of the activity PDF for densities $\rho = 1/2$ and $1/4$, and varying system sizes L. Results are given in Table III, together with the theoretical predictions summarized in Eqs. (51)–(53). Similarly to the open boundary case, the agreement is very good, except that accuracy for the skewness is comparatively low. For $\rho = 1/2$, in particular, comparison of simulational data with predicted values of skewness [see Eq. (58)] is difficult because the latter are rather small.

We then made long runs with $N_{\rm sam} = 10^7$ for $L = 16$ for both $\rho = 1/2$ and $1/4$, with the results displayed in Table IV. In this case, the numerical results clearly confirm the theoretical prediction for the skewness: very accurately for $\rho = 1/4$, and within reasonable error bars for $\rho = 1/2$.

As a consequence of Eq. (57), for $\rho \neq 1/2$ the skewness of the PDFs for PBC tends to grow, in absolute value, as $|\rho - 1/2|$ increases. For system sizes L large enough, so that the set of (discrete) allowed activity values can be reasonably well represented as a continuum, one can approximate the respective PDF by a Gaussian with a skew-inducing perturbation:

$$P(x) = \left[1 + a\left(\frac{x'}{\sigma}\right)^3\right] G(x', \sigma), \tag{59}$$

TABLE III. For systems with PBC, L sites, and ρ as specified, $\langle a_L\rangle \equiv \langle A\rangle/L$ is average current activity [normalized as in Eq. (3)]; $\Delta \equiv [\langle a_L^2\rangle - \langle a_L\rangle^2]^{1/2}$; Th stands for results from theory [Eqs. (51)–(53)], and N for results of numerical simulations with $N_{\rm sam} = 10^6$, $N_{\rm set} = 10$ (see text).

L	Type	$\langle a_L\rangle$	Δ	Skew
		$\rho = 1/2$		
64	Th	0.253968 . . .	0.0312461 . . .	0.000130123 . . .
	N	0.25398(2)	0.031261(20)	− 0.0005(19)
128	Th	0.251969 . . .	0.0220964 . . .	0.000022272 . . .
	N	0.25197(2)	0.022095(11)	0.0004(17)
256	Th	0.250980 . . .	0.0156249 . . .	0.000003875 . . .
	N	0.25099(1)	0.015629(10)	0.0001(26)
		$\rho = 1/4$		
64	Th	0.190476 . . .	0.0231771 . . .	− 0.17946 . . .
	N	0.19048(2)	0.023178(11)	− 0.1799(13)
128	Th	0.188976 . . .	0.0164837 . . .	− 0.12226 . . .
	N	0.18898(1)	0.016492(10)	− 0.1237(30)
256	Th	0.188235 . . .	0.0116877 . . .	− 0.08487 . . .
	N	0.18823(1)	0.011690(7)	− 0.0833(29)

where $x' \equiv x - x_0$, $G(x',\sigma)$ is a Gaussian curve centered at $x = x_0$, with width σ; a, x_0, and σ are adjustable parameters, with the proviso $|a| \ll 1$.

In Fig. 5, we show the results of fitting data for $L = 256$, $\rho = 1/4$ to Eq. (59). The adjusted estimate of $a = -0.0120(25)$ corresponds to $S = -0.072(15)$, which compares favorably with the values given in Table III, albeit with a somewhat large uncertainty. The adjusted width $\sigma = 0.01171(3)$ is in very good agreement with the Δ values (both from theory and from numerics) given in the same table.

For a graphic illustration of large skewness with PBC (similar to the effect shown in Fig. 3 for open BC with $\alpha \ll 1$, $\beta \approx 1$), one needs $|\rho - 1/2|$ large, as well as large L. In the low-density regime, the maximum allowed activity is $A_{\rm max} = M$, M being the number of particles in the system. One has, from Eq. (51), $\langle A\rangle = M(1-\rho)[1 + \mathcal{O}(L^{-1})]$, thus the maximum allowed value of $x = (A - \langle A\rangle)/L$ is $\rho^2[1 + \mathcal{O}(L^{-1})]$. This is illustrated in Fig. 6, for $\rho = 1/16$ and various values of (large) L, where the sharp cutoff in the forward end of the PDF is evident. For the curves shown, the calculated values of the skewness are $S = -0.58963\ldots$, $-0.41258\ldots$, and $-0.29023\ldots$, respectively, for $L = 512$, 1024, and 2048

TABLE IV. For systems with PBC, $L = 16$ sites, and ρ as specified, $\langle a_L\rangle \equiv \langle A\rangle/L$ is average current activity [normalized as in Eq. (3)]; $\Delta \equiv [\langle a_L^2\rangle - \langle a_L\rangle^2]^{1/2}$; Th stands for results from theory [Eqs. (51)–(53)], and N for results of numerical simulations with $N_{\rm sam} = 10^7$, $N_{\rm set} = 10$ (see text).

Type	$\langle a_L\rangle$	Δ	Skew
	$\rho = 1/2$		
Th	0.266667 . . .	0.0623610 . . .	0.005140 . . .
N	0.26668(1)	0.062350(8)	0.00515(72)
	$\rho = 1/4$		
Th	1/5	0.0443203 . . .	− 0.455600 . . .
N	0.20002(1)	0.044313(4)	− 0.45578(30)

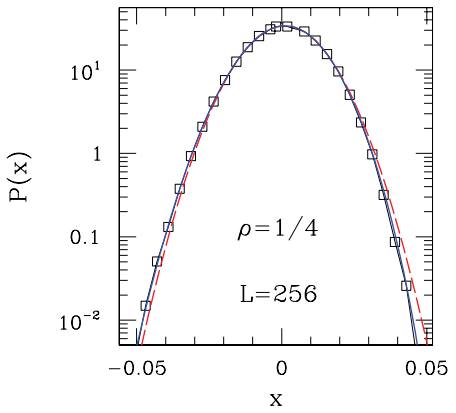

FIG. 5. (Color online) PDF for the reduced variable $x \equiv (A - \langle A\rangle)/L$ for system with PBC, $\rho = 1/4$, $L = 256$ [see Eq. (3)]. The points are from numerical simulations $N_{\rm sam} = 10^6$ samples. The full (blue) line is the perturbed Gaussian distribution given by Eq. (59), adjusted to the numerical data. The dashed (red) line is a pure Gaussian fit to the same data, and is shown for reference.

[see Eqs. (51)–(53)]. The low-density regime with PBC is thus the counterpart of the small-α, large-β example for open BC of Sec. III B. Note that the skewness here has the opposite sign to that case.

We considered the system with $\rho = 1/16$, $L = 2048$ in further detail. Figure 7 shows the results of numerical simulations, as well as their best fit to Eq. (59). The adjusted value of $a = -0.043(9)$ corresponds to $S = -0.27(6)$, in broad agreement with the theoretical prediction. However, it can be seen that the perturbative scheme of Eq. (59) can not properly account for the long tail at negative x. Although we have checked that the tail still varies as $\sim \exp[-b(x - x_0)^2]$, it is not possible to find a single set of parameters in Eq. (59) which optimizes the fit to the latter region, without seriously compromising the description of data away from the tail.

In Ref. [22], an approach similar to the one described above was used to calculate current activity PDFs for one-dimensional flow of extended objects with exclusion, on a ring.

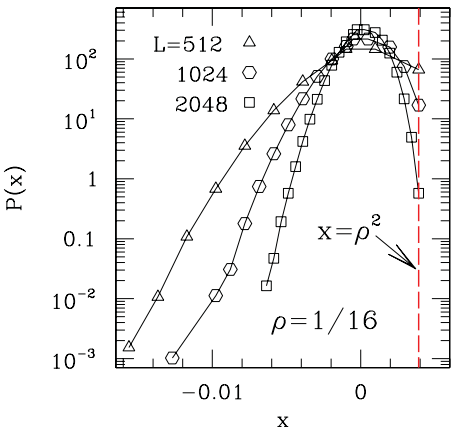

FIG. 6. (Color online) PDFs for the reduced variable $x \equiv (A - \langle A\rangle)/L$ for systems with PBC, $\rho = 1/16$, and sizes L as specified [see Eq. (3)]. The points are from numerical simulations $N_{\rm sam} = 10^6$ samples. The dashed (red) line corresponds to the maximum allowed activity (apart from small corrections of order L^{-1}, see text).

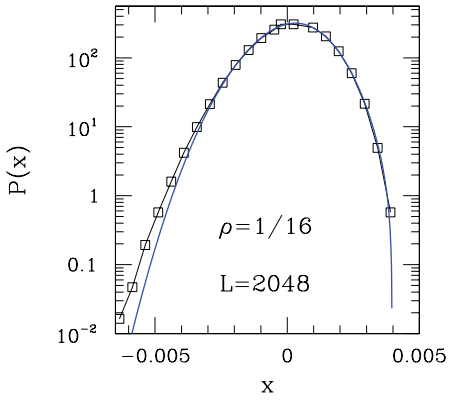

FIG. 7. (Color online) PDF for the reduced variable $x \equiv (A - \langle A \rangle)/L$ for system with PBC, $\rho = 1/16$, $L = 2048$ [see Eq. (3)]. The points are from numerical simulations $N_{\rm sam} = 10^6$ samples. The full (blue) line is the perturbed Gaussian distribution given by Eq. (59), adjusted to the numerical data.

Those were compared to results of numerical simulations of the same quantity, with very good agreement (see their Fig. 1). Note that their system of extended objects corresponds to an effective lattice of $L = 35$ sites with $M = 15$ point particles. For this case, Eqs. (51)–(53) give, e.g., $S = -0.015\ldots$. So, this is a regime where deviations from Gaussianity are rather small for activity distributions, which is visually confirmed by the aspect of their figure referred to above.

IV. DISCUSSION AND CONCLUSIONS

The investigation of current fluctuations is usually carried out by examining the total charge crossing a given bond, during a long time interval in the steady-state regime [7–13]. Conversely, the snapshot nature of current activity means that samples are collected at a fixed time; in this case, the nontrivial features arise when one considers the corresponding global quantity, i.e., the sum of contributions from all bonds in the system, at a given instant. When focusing on fluctuations of either quantity, the task for currents is made more involved by the need to subtract a background term which grows linearly in time, and (depending on the specifics of the case) additional sublinear terms as well. Current-activity fluctuations, on the other hand, can be adequately sampled by resorting to large enough systems, so that discrete-lattice effects are minimized. While, as emphasized earlier, these two quantities are distinct in character, both can yield physical insights into the properties of flow with exclusion.

The results of the numerical simulations, reported in Sec. III, provide unequivocal support to the predictions summarized in Eqs. (29)–(31) [for the cases where Eqs. (33) and (34) apply], and in Eqs. (51)–(53). We thus collected further information, regarding points of the α-β phase diagram for open BC not investigated in Sec. III, by applying the general expression for the quantities Z_L [Eq. (32)] directly to Eqs. (29)–(31). The results are as follows.

We focused on the large-L dependence of the cumulants C_n, $n = 1 - 3$, as reflected in the associated quantities $\Delta = C_2^{1/2}/(L+1)$ and $S = C_3/C_2^{3/2}$, as well as on the sign of the latter. From numerical evaluations of Eqs. (29)–(31)

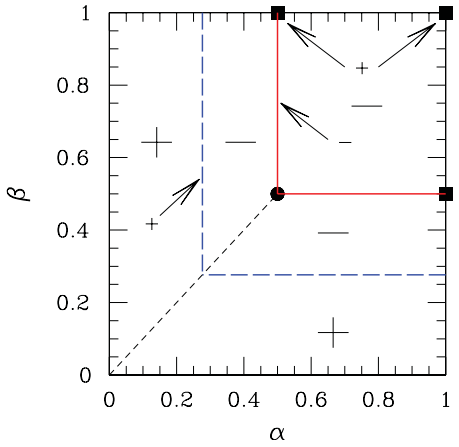

FIG. 8. (Color online) The sign of skewness S in the various regions of the α-β phase diagram is shown. The large-L dependence $|S| \propto L^{-x}$ is in the low-current phases [$\alpha < 1/2$, β and $\beta < 1/2$, α] $x = 1/2$, except for the long-dashed (blue) lines, including their extremes at $\beta = 1$ and $\alpha = 1$ [$x = 3/2$] (see text for explanation of these lines). In the high-current phase α, $\beta > 1/2$, $x = 3/2$. Full (red) lines separating high- and low-current phases: $x = 3/2$. Full squares: $x = 5/2$. On the $\alpha = 1$ and $\beta = 1$ lines, S has the same sign and L dependence as in the respective adjacent regions, except for the points marked by full squares. The circle marks $(\alpha,\beta) = (1/2,1/2)$ where $S \equiv 0$ [see Eq. (17)]. The short-dashed line is the coexistence line between high-and low-density phases. Because of particle-hole duality, S is the same for pairs of points symmetric with respect to the $\alpha = \beta$ line.

using Eq. (32) we found $\Delta \propto L^{-1/2}$ everywhere, and strong evidence for

$$S \propto L^{-k_m - 3/2} \tag{60}$$

in the limit of large L, where $k_m = -1$ for some extended regions of the α-β phase diagram, $k_m = 0$ for other regions, as well as special lines, and $k_m = 1$ for some special points (see Fig. 8). Equation (60) corresponds to $C_3 \propto L^{-k_m}$ at large L. All this is consistent with results obtained by using in Eqs. (29)–(31), instead of Eq. (32) for Z_L, the asymptotic approximations to it provided by Refs. [3,14,15] [see, e.g., Eqs. (8) and (9) of Ref. [15]]. This gives, for the low-current phases [$\alpha < 1/2$, β (low density) or $\beta < 1/2$, α (high density)] and the coexistence line ($\alpha = \beta < 1/2$) the results

$$\begin{aligned} C_2 &= L\mu(1-3\mu) + \mathcal{O}(1), \\ C_3 &= L\mu(1-4\mu)(1-5\mu) + \mathcal{O}(1), \end{aligned} \tag{61}$$

where $\mu = \min(\alpha,\beta)\,[1 - \min(\alpha,\beta)]$. Thus, in these cases, away from the dual lines $\mu = 1/5$ the large-L skewness is $S \propto L^{-1/2}$ and positive (negative) for μ less (greater) than $1/5$. At $\mu = 1/5$, corresponding to $\min(\alpha,\beta) = \frac{1}{2} - \frac{\sqrt{5}}{10} = 0.27639\ldots$, the vanishing of the $\mathcal{O}(L)$ term in C_3 makes $|S| \leqslant \mathcal{O}(L^{-3/2})$. These agree with the signs and L dependences of S from the numerical calculations using Eq. (32), gathered in Fig. 8. There, the long-dashed lines are the dual lines where $\mu = 1/5$. They cross the $\alpha + \beta = 1$ line at $\alpha\beta = 1/5$. At this point, the term in C_3 contributing to $S \propto L^{-1/2}$ indeed vanishes, as anticipated in Eq. (16). In fact, Eqs. (61) reproduce Eqs. (15) and (16), everywhere along the $\alpha + \beta = 1$ line,

including $\alpha = \beta = 1/2$ where, from Sec. II A, we know that S vanishes.

For α, β inside the high-current phase boundaries, using the asymptotic Z_L [Eq. (8) of Ref. [15]] in Eqs. (29)–(31) gives $S \propto L^{-3/2}$, in agreement with the results obtained using the full form [Eq. (32)]. Furthermore, the full form shows that near $(\alpha,\beta) = (\frac{1}{2},\frac{1}{2})$, $S > 0$ for small L, crossing over to negative values as L increases. For example, at $\alpha = \beta = 0.55$, S goes through zero for $L \approx 300$. The $L^{-3/2}$ dependence involves an exception to the normal subdominance of injection and ejection contributions: both the approximate and exact procedures show that without the injection and ejection contribution [i.e., considering the $\langle A'^n \rangle$ of Eqs. (29)–(31)], S would have been $\mathcal{O}(L^{-5/2})$; an associated relationship to cumulants of A' helps to explain the result $S \propto L^{-5/2}$ at the special boundary point $\alpha = \beta = 1$ [see Eq. (35)].

It is remarkable that the asymptotic approximations for Z_L are sufficiently accurate, when inserted in Eqs. (29)–(31), to give the correct asymptotics for the cumulants and skewness, given the high orders of cancellations in $1/L$ expansions often occurring. Direct calculation of activity cumulants using asymptotic PDFs given at the end of Sec. II B3 are less accurate: for example, the Laplace approximation mentioned there gives, inside the low-current phases, $S \propto L^{-3/2}$, but does not give the crossover near the long-dashed (blue) lines of Fig. 8.

Correspondence with select results for standard current studies is as follows. In Ref. [10], current statistics were considered for open BC. At large L, for the PDF of total charge fluctuations, $\widetilde{Q} = Q(T) - \langle Q(T) \rangle$, accumulated up to time T they found critical scaling at $\alpha = \beta = 1/2$ with $T^{1/2z} P_T(\widetilde{Q}) = f(\widetilde{Q}/T^{1/2z})$, $z = 3/2$; elsewhere on the $\alpha + \beta = 1$ line, scaling of the PDF was found to be Gaussian. Although their results are strictly not comparable to ours, their Fig. 4 suggests that, e.g., for $L = 256$ critical scaling would only persist up to times $T \lesssim 3000$. Whether or not some such signature would show up in the (fixed-time) statistics of current activity, for times other than those used in this work is an open question.

Second, in Ref. [12] it was found that, at the special point $\alpha = \beta = 1$, C_3 approaches a small, finite (negative) value, as $L \to \infty$. On the other hand, their $C_2 \propto L^{-1/2}$. Thus, the standard skewness [20] would become very large for large L. Here, in contrast, the skewness of the current activity approaches zero as $L \to \infty$ everywhere. Furthermore, it is positive at the above-mentioned special point. This implies that any relationship of current fluctuations to those of the activity would involve subtle features.

ACKNOWLEDGMENTS

The authors thank F. Essler for helpful discussions. S.L.A.d.Q. thanks the Rudolf Peierls Centre for Theoretical Physics, Oxford, where most of this work was carried out, for the hospitality, and CAPES for funding his visit. The research of S.L.A.d.Q. is financed by the Brazilian agencies CAPES (Grant No. 0940-10-0), CNPq (Grant No. 302924/2009-4), and FAPERJ (Grant No. E-26/101.572/2010).

APPENDIX A: TRANSFER MATRIX RESULTS FOR $\alpha + \beta = 1$

The evaluation of Eq. (9) using the representation in which T is diagonal yields

$$\langle e^{\lambda A} \rangle = a_+ \mu_+^{L-1} + a_- \mu_-^{L-1}, \tag{A1}$$

where

$$\mu_\pm = \mu_\pm(\lambda) = \tfrac{1}{2}[1 \pm \sqrt{1 + 4\alpha\beta\gamma}] \quad (\gamma \equiv e^\lambda - 1) \tag{A2}$$

and

$$a_\pm(\lambda) = [(\alpha\, e^{\lambda\beta} + \beta)\mu_\pm + \alpha\beta\gamma] \, \frac{[\mu_\pm + \beta(e^{\lambda\alpha} - 1)]}{[(2\mu_\pm - 1)\mu_\pm]}. \tag{A3}$$

The first three derivatives of $\ln\langle e^{\lambda A} \rangle$ at $\lambda = 0$ then provide the following leading cumulants [exploiting $\mu_+(0) = 1$, $\mu_-(0) = 0$]:

$$\begin{aligned} &C_1 = (L+1)\,\alpha\beta, \quad C_2 = L\,\alpha\beta - (3L+1)\,(\alpha\beta)^2, \\ &C_3 = L\,\alpha\beta - (9L-1)\,(\alpha\beta)^2 + 4(5L-1)\,(\alpha\beta)^3. \end{aligned} \tag{A4}$$

These results generalize Eqs. (14)–(16) and show that Eqs. (14)–(16) apply for $L \gg 1$, $\alpha\beta/(1-3\alpha\beta)$, $\alpha\beta/(1-5\alpha\beta)$, respectively. The exact cumulants given above can alternatively be obtained from the forms provided for general α, β in Sec. II B1, taking Eq. (33) into account.

APPENDIX B: $\langle A'^3 \rangle$, $\langle A^3 \rangle$ FOR GENERAL α, β

We first consider the product of bond terms

$$\begin{aligned} A'^3 &= \sum_{\ell=1}^{L-1} (1-\zeta_\ell)\,\zeta_{\ell+1} \sum_{m=1}^{L-1} (1-\zeta_m)\,\zeta_{m+1} \sum_{n=1}^{L-1} (1-\zeta_n)\,\zeta_{n+1} \\ &\equiv \sum_{\ell m n} T_{\ell m n}. \end{aligned} \tag{B1}$$

(ℓ, m, n) identifies a particular term in the triple sum, and corresponds to a point in an $(L-1) \times (L-1) \times (L-1)$ cube in three-dimensional $\ell\, m\, n$ space.

We need to distinguish and enumerate the following cases (a)–(f), of which (a)–(e) involve repeated site labels:

(a) $(\ell\, m\, n) = (\ell,\ell,\ell)$, $1 \leqslant \ell \leqslant L-1$: $N_a = L-1$ points (on the diagonal of the cube). $T_{\ell\ell\ell} = (1-\zeta_\ell)^3\,\zeta_{\ell+1}^3 = (1-\zeta_\ell)\,\zeta_{\ell+1}$.

(b) $(\ell\, m\, n) = (\ell,\ell,\ell+1)$, $1 \leqslant \ell \leqslant L-2$: $L-2$ points (on subdiagonal line). $T_{\ell\ell\ell+1} = (1-\zeta_\ell)^2\,\zeta_{\ell+1}^2\,(1-\zeta_{\ell+1})\,\zeta_{\ell+2} = 0$. This is one example out of six lines of the type $(\ell\, m\, n) = (\ell,\ell,\ell \pm 1)$ and cyclic variations, containing altogether $N_b = 6(N-2)$ points, each giving zero contribution.

(c) $(\ell\, m\, n) = (\ell,\ell \pm 1,\ell \mp 1)$, ($\ell$ varying; ℓ, m, n all different): With cyclic variations, there are six lines containing points of this type, altogether making $N_c = 6(L-3)$ points, all with $T_{\ell m n} = 0$.

(d) $(\ell\, m\, m)$: As ℓ, m vary, this corresponds to a plane slicing the cube. It contains $(L-1)^2$ points of which $L-1$ are on the line $(\ell\, m\, n) = (\ell,\ell,\ell)$ specified in (a), and $2(L-2)$ are

on lines $(\ell,\ell\pm1,\ell\pm1)$ of the type specified in (b). So, there are $(L-1)^2-[L-1+2(L-2)]$ "new" points associated with the plane. Allowing for cyclic variations, there are three such planes, containing altogether $N_d=3(L-2)(L-3)$ new points, each with $T_{\ell m m}=(1-\zeta_\ell)\,\zeta_{\ell+1}\,(1-\zeta_m)\,\zeta_{m+1}$ ($m\neq\ell$, $\ell\pm1$).

(e) $(\ell,m,m\pm1)$ with ℓ, m varying (and cyclic variations). There are six planes of this type. Discounting points already accounted for, the new planes contain a total of $N_e=6(L-3)(L-4)$ new points, at each of which $T_{\ell m n}$ vanishes.

(f) The remaining points $(\ell\,m\,n)$ have no pair of coordinates equal or differing by ±1, so the associated $T_{\ell m n}$ has no shared site labels. The total number of such points is $N_f=(L-1)^3-(N_a+N_b+N_c+N_d+N_e)=(L-3)(L-4)(L-5)$.

The average of the addition of the nonzero contributions to A'^3 from (a), (d), and (f) gives

$$\begin{aligned}\langle A'^3\rangle &= N_a\,\langle(1-\zeta_\ell)\,\zeta_{\ell+1}\rangle\\ &\quad+N_d\,\langle(1-\zeta_\ell)\,\zeta_{\ell+1}(1-\zeta_m)\,\zeta_{m+1}\rangle\\ &\quad+N_f\,\langle(1-\zeta_\ell)\,\zeta_{\ell+1}(1-\zeta_m)\,\zeta_{m+1}\,(1-\zeta_n)\,\zeta_{n+1}\rangle.\end{aligned}\tag{B2}$$

Here, no pair from $\ell\,m\,n$ are equal or differ by ±1, so we can reduce Eq. (B2) using Eqs. (23) and (25), and their generalization for this case

$$\langle(1-\zeta_\ell)\,\zeta_{\ell+1}\,(1-\zeta_m)\,\zeta_{m+1}\,(1-\zeta_n)\,\zeta_{n+1}\rangle=\frac{Z_{L-3}}{Z_L}.\tag{B3}$$

We find

$$\begin{aligned}\langle A'^3\rangle &= (L-3)(L-4)(L-5)\,\frac{Z_{L-3}}{Z_L}\\ &\quad+3(L-2)(L-3)\,\frac{Z_{L-2}}{Z_L}+(L-1)\,\frac{Z_{L-1}}{Z_L}.\end{aligned}\tag{B4}$$

The generalization for inclusion of injection and ejection contributions in the third moment of the activity involves similar steps to those for the second moment, given in Eq. (27). We first write

$$A^3=T_0+3T_1+3T_2+T_3,\tag{B5}$$

where

$$T_n=(A')^n\,[\alpha\,\zeta_1+\beta\,(1-\zeta_L)]^{3-n}.\tag{B6}$$

Using $(\alpha\,\zeta_1)^m=\alpha^m\,\zeta_1$, $(\alpha\,\zeta_1)^m\,(1-\zeta_1)\,\zeta_2=0$ $(m\geqslant1)$ and similarly for $\beta\,(1-\zeta_L)$, one finds

$$\begin{aligned}\langle T_0\rangle &= (\alpha^2+\beta^2)\,\frac{Z_{L-1}}{Z_L}+3(\alpha+\beta)\,\frac{Z_{L-2}}{Z_L},\\ \langle T_1\rangle &= (L-2)(\alpha+\beta)\,\frac{Z_{L-2}}{Z_L}+2(L-3)\,\frac{Z_{L-3}}{Z_L},\\ \langle T_2\rangle &= 2(L-2)\,\frac{Z_{L-2}}{Z_L}+2(L-3)(L-4)\,\frac{Z_{L-3}}{Z_L}.\end{aligned}\tag{B7}$$

With $\langle T_3\rangle=\langle A'^3\rangle$ from Eq. (B4),

$$\begin{aligned}\langle A^3\rangle &= (L-1)(L-2)(L-3)\,\frac{Z_{L-3}}{Z_L}\\ &\quad+3(L-1)(L-2+\alpha+\beta)\,\frac{Z_{L-2}}{Z_L}\\ &\quad+(L-1+\alpha^2+\beta^2)\,\frac{Z_{L-1}}{Z_L}.\end{aligned}\tag{B8}$$

APPENDIX C: $\langle A^3\rangle$ FOR PBC

Along similar lines to those followed in Appendix B, we consider the product

$$A^3=\sum_{\ell=1}^{L}(1-\zeta_\ell)\,\zeta_{\ell+1}\sum_{m=1}^{L}(1-\zeta_m)\,\zeta_{m+1}\sum_{n=1}^{L}(1-\zeta_n)\,\zeta_{n+1},\tag{C1}$$

with $\zeta_{L+1}\equiv\zeta_1$.

The cases involving site labels are the same set (a)–(f) described in Appendix B; only the enumerations vary. Recalling Eq. (B2), one has now, adding up the nonzero contributions,

$$\begin{aligned}\langle A^3\rangle &= N_a^p\,\langle(1-\zeta_\ell)\,\zeta_{\ell+1}\rangle\\ &\quad+N_d^p\,\langle(1-\zeta_\ell)\,\zeta_{\ell+1}(1-\zeta_m)\,\zeta_{m+1}\rangle\\ &\quad+N_f^p\,\langle(1-\zeta_\ell)\,\zeta_{\ell+1}(1-\zeta_m)\,\zeta_{m+1}\,(1-\zeta_n)\,\zeta_{n+1}\rangle.\end{aligned}\tag{C2}$$

The numerical coefficients are as follows:

(a) $(\ell\,m\,n)=(\ell,\ell,\ell)$, $1\leqslant\ell\leqslant L$: $N_a^p=L$ points.

(d) $(\ell\,m\,m)$: $N_d^p=3L(L-3)$ points.

(f) The points $(\ell\,m\,n)$, which have no pair of coordinates equal or differing by ±1: $N_f^p=L(L-4)(L-5)$ points.

One has

$$\langle(1-\zeta_\ell)\,\zeta_{\ell+1}\rangle=\frac{{}_{L-2}C_{M-1}}{{}_LC_M},\tag{C3}$$

$$\langle(1-\zeta_\ell)\,\zeta_{\ell+1}(1-\zeta_m)\,\zeta_{m+1}\rangle=\frac{{}_{L-4}C_{M-2}}{{}_LC_M},\tag{C4}$$

$$\langle(1-\zeta_\ell)\,\zeta_{\ell+1}\,(1-\zeta_m)\,\zeta_{m+1}\,(1-\zeta_n)\,\zeta_{n+1}\rangle=\frac{{}_{L-6}C_{M-3}}{{}_LC_M}.\tag{C5}$$

So, recalling Eq. (50),

$$\langle A^3\rangle=a_0\,(1+3a_1+a_1\,a_2).\tag{C6}$$

[1] B. Derrida, Phys. Rep. **301**, 65 (1998).

[2] G. M. Schütz, in *Phase Transitions and Critical Phenomena*, edited by C. Domb and J. L. Lebowitz (Academic, New York, 2000), Vol. 19.

[3] B. Derrida, M. Evans, V. Hakim, and V. Pasquier, J. Phys. A: Math. Gen. **26**, 1493 (1993).

[4] R. B. Stinchcombe, Adv. Phys. **50**, 431 (2001).

[5] R. A. Blythe and M. R. Evans, J. Phys. A: Math. Gen. **40**, R333 (2007).
[6] B. Derrida, M. R. Evans, and D. Mukamel, J. Phys. A: Math. Gen. **26**, 4911 (1993).
[7] B. Derrida, M. R. Evans, and K. Mallick, J. Stat. Phys. **79**, 833 (1995).
[8] B. Derrida and J. L. Lebowitz, Phys. Rev. Lett. **80**, 209 (1998).
[9] T. Bodineau and B. Derrida, J. Stat. Phys. **123**, 277 (2006).
[10] T. Karzig and F. von Oppen, Phys. Rev. B **81**, 045317 (2010).
[11] M. Gorissen and C. Vanderzande, J. Phys. A: Math. Gen. **44**, 115005 (2011).
[12] A. Lazarescu and K. Mallick, J. Phys. A: Math. Gen. **44**, 315001 (2011).
[13] J. de Gier and F. H. L. Essler, Phys. Rev. Lett. **107**, 010602 (2011).
[14] M. Depken and R. Stinchcombe, Phys. Rev. Lett. **93**, 040602 (2004).
[15] M. Depken and R. Stinchcombe, Phys. Rev. E **71**, 036120 (2005).
[16] S. L. A. de Queiroz and R. B. Stinchcombe, Phys. Rev. E **78**, 031106 (2008).
[17] Z. Nagy, C. Appert, and L. Santen, J. Stat. Phys. **109**, 623 (2002).
[18] J. de Gier and F. H. L. Essler, Phys. Rev. Lett. **95**, 240601 (2005); J. Stat. Mech.: Theor. Exp. (2006) P12011.
[19] R. B. Stinchcombe and G. M. Schütz, Phys. Rev. Lett. **75**, 140 (1995).
[20] W. Press, B. Flannery, S. Teukolsky, and W. Vetterling, *Numerical Recipes in Fortran, The Art of Scientific Computing*, 2nd ed. (Cambridge University Press, Cambridge, England, 1992), Chap 14.
[21] S. L. A. de Queiroz and R. B. Stinchcombe, Phys. Rev. E **54**, 190 (1996).
[22] L. B. Shaw, R. K. P. Zia, and K. H. Lee, Phys. Rev. E **68**, 021910 (2003).